ALMA MATER STUDIORUM
UNIVERSITÀ DI BOLOGNA

SCHOOL OF ENGINEERING

Department of
Electrical, Electronic and Information Engineering
"Guglielmo Marconi"
DEI

Master's Degree in Automation Engineering

Master Thesis
in
Optimal Control

Control of an autonomous aerodynamic airshield for training Olympic 100m sprint athletes

Candidate:
Giulia Cutini

Supervisor:
Prof. Giuseppe Notarstefano

Co-supervisor:
Prof. Melanie Zeilinger
Dr. Andrea Carron
Ing. Lorenzo Sforni

Academic Year
2022–2023

Session
III

Abstract

Contents

Introduction

Motivations

In recent decades, the integration of advanced technologies has become an integral facet of sport, introducing a new era of innovation and performance enhancement [1]. In sports characterized by high-speed competition, where victories are often determined by fractions of a second, the advancements in technology have revolutionized performance across various disciplines.

The development of streamlined swimsuits with advanced materials reduces drag and enhances buoyancy, leading to faster times in competitive swimming events. Ski manufacturers utilize materials like carbon fiber and titanium in ski construction, resulting in lighter yet more stable skis that offer better control and responsiveness on the slopes. The incorporation of carbon fiber also into athletic footwear has not only reduced weight but also enhanced energy return and propulsion, while concurrently reducing the risk of injury.

The exploitation of technology for improving performances is not only used for competitions but also during the training phase. In the track and field context, several training techniques have been used for the enhancement of running speed. Among several possibilities overspeed training involves performing exercises or movements at a velocity higher than what the athlete can achieve through voluntary effort in classical environmental conditions. Many methods for experience supramaximal velocities during trainings have been proposed: the usage of assistance mechanisms such as bungee cords or sleds is analized in [2] and is found to be potentially dangerous for sprinters, requiring body contact with an external tool. Performing sprints on a downward slope allows to accelerate beyond typical maximal speed due to assistance provided to gravity force [3].

In the context of gaining a training edge in sprint events the concept of aerodynamic drag resistance assumes a great importance. Accordingly sprinters meticulously refine their body position, posture, and apparel to minimize aerodynamic drag. For this reason CONI (Italian National Olympic Committee) Institute of Sports Science presented in 2021 an aerodynamic shield to drastically reduce the resistance to forward movement during sprinters' training [4]. This shield allows athletes to run in the slipstream behind a car pulling the shield, experiencing speeds higher than those of the competition but with the same power output.

Advancement in automated driving technology has created opportunities for many fields and autonomous vehicles (AVs) have become increasingly prevalent. Given their versatility and potential to enhance efficiency and convenience, it's natural to consider their application in the realm of sports. Similarly to the user-cooperative robots, designed to stay in direct contact with humans and assist them in several situations, an autonomous vehicle has been designed for driving the aerodynamic airshield. Furthermore, intelligent control algorithms have shown huge advantages in autonomous system control, taking into account factors such as control error, bound constraints on system actuators, disturbance rejection and safety guarantees. Additionally, control algorithms can be designed to continuously monitor and analyze data from various sensors in real-time, enabling them to detect and respond to potential hazards or deviations from safety protocols more effectively than human operators.

This thesis is the result of an abroad internship in ETH (Eidgenössische Technische Hochschule) Zürich, with the purpose of designing a proper controller to regulate an autonomous go-kart pulling a plexiglass airshield, according to the runner behaviour.

Literature

Numerous control techniques have been used in the last decades to enhance the efficiency of AVs in several different contexts. Longitudinal control of automated vehicles has received attention since the 1960s, and possibly even earlier. In [5] an historical review of advanced vehicle control systems and longitudinal control of automated vehicles is presented. The control of vehicle acceleration to achieve a desired speed profile, essential keypoint of longitudinal control, is the main purpose of this thesis.

The initial and simplest approach adopted to control the go-kart, which must maintain a constant reference position and velocity, relative to the runner behind it, involved a cascade of two Proportional-Integral-Derivative (PID) controllers. The first PID controller regulates the kart's position and generates a reference velocity for the second controller, a velocity PID.

While PID controllers are widely used in industrial applications due to their straightforward implementation, they were not the optimal choice for this application. The main challenges of this control scheme includes difficulty in parameter tuning, in handling multi-variable processing and in addressing the initial phase of motion, where the runner's acceleration exceeds the kart's maximum capability, together with the impossibility of predicting the future motion of vehicle.

The application requires the go-kart to maintain a consistent desired position and velocity relative to the runner. This task is quite similar to adaptive cruise control (ACC), where the goal is to maintain a safe distance from the vehicle ahead while also adjusting the speed to match changing traffic conditions.

Thanks to the capability of optimal controllers to cover multiple objectives and to predict future vehicle behaviour, Linear Quadratic Regulator (LQR) and Model Predictive Control (MPC) have been widely used for vehicle control in interacting contexts. In [6] distance and relative velocity between preceding and controlled vehicles are used as states to design an LQR controller that gives acceleration of the controlled vehicle as input, in such a way to minimize a proper cost function. Model Predictive Control is also largely used thanks to its capability of controlling a multi-variable process while satisfying a set of state and input constraints. According to [7] the essential elements of this controller are a prediction model that allows future predictions, the definition of an objective function reflecting the desired system behaviour, and constraints on both state and input. In the framework of MPC for adaptive cruise control, in [8] the same state and input variables than in [6] are used but constraints can be also incorporated. Differently, in [9] the controlled vehicle velocity is added as a third state and the acceleration of the preceding vehicle is included in the prediction model, regarded as an unknown external disturbance.

The MPC approach is strongly model-based in the sense that uses a model of the system to produce a prediction of system behaviour. The presence of uncertainties on this model may lead to unsatisfying results of the control task. For this reason [10], [11] show offset-free MPC formulations able to achieve output tracking of reference signals despite the presence of Model-Plant Mismatch (MPM). For this purpose an augmented predictive model added with an artificial constant disturbance that represents modeling uncertainties, is used. To estimate both state ad disturbance from output measurements a disturbance observer must be properly designed and added in conjunction with feedback control law. Accordingly to [12] by appropriately including a disturbance estimate in a control law, MPM effects can be approximately removed in steady-state and offset-free tracking of constant references can be achieved.

Contributions

The main contribution of this thesis lies in the analysis and implementation of linear controllers for a pioneering autonomous driving go-kart, which is utilized for towing the airshield during the training of Olympic athletes participating in the 100m event. Specifically, the thesis proposes and compares two different control schemes in terms of performances and control architecture.

Initially, a non linear model that accurately captures the dynamics of the kart with the airshield attached is identified. Later a good linear approximation is found and used as basis for the design of the predictive controllers. The first step in control development involves the design of a Linear Quadratic Regulator (LQR) with a gain scheduling approach, where Q and R parameters vary depending on the motion phase. This gain scheduling approach addresses the challenges associated with the different maximum accelerations of the kart and of the runner in the first phase of the motion. Subsequently, a Model Predictive Control (MPC) is designed with the purpose of incorporate information on the runner future expected behaviour into the linear prediction model. Furthermore, since MPC is highly model based a disturbance observer and Offset-free MPC has been implemented with the purpose of increasing the accuracy of the predictive model and to obtain a zero-offset in tracking peace-wise affine (PWA) reference trajectories.

The depicted workflow highlights how the control scheme architecture has been simplified starting from the two control loops governing the cascade of PID controllers. The gain scheduling LQR, which switches between two different control gains depending on the motion phase, just makes use of two different regulators. Ultimately, this thesis culminates in a single MPC controller capable of governing the system under all possible operating conditions, integrating information about the future evolution of the runner's velocity profile into the prediction model to further enhance tracking performance.

Both controllers have been developed and tested in simulation using Python and on the real system using ROS2.

Organization

This section provides to the reader a guide to the organization of the thesis.

In Chapter 1 a theoretical background and an overview of the fundamental methodologies used in the control design are presented.

Chapter 2 is focused on discussing the problem set-up, the formulation of the optimal control techniques developed to accomplish the desired task, in particular the Linear Quadratic Regulator (LQR) and the Model Predictive Control (MPC), in the specific context of this application.

Chapter 3 gives a description of the system mechanical structure, hardware and sensors. Then it shows the numerical results of the controllers application obtained both in Python simulation and on the real hardware. A comparison of the performance in different scenarios is also presented. This demonstrate the effectiveness of the proposed methodologies.

Chapter 1

Optimal Control theory for controlling dynamical systems via Linear Quadratic Regulator and Model Predictive Control

In this chapter the aim is to provide the necessary optimal control theoretical background before introducing the design process and the main peculiarities and limitations of the implemented controllers: the Linear Quadratic Regulator (LQR) and the Model Predictive Control (MPC).

Optimal control theory provides a mathematical framework for addressing control theory problems by optimizing control laws with respect to given cost functions, in order to achieve optimal system regulation.

Such theoretical analysis is essential for fully comprehending the features and performance of the LQR and MPC controllers discussed in Chapter 2 within the specific context of the considered application.

1.1 Linear Quadratic Regulator

In 1960, Kalman introduced for the first time the linear-quadratic feedback control, which later evolved into the Linear Quadratic Regulator (LQR) [13] in the continuous-time context. The LQR is a feedback control algorithm designed to stabilize and optimize the performance in case where the dynamical system can be described by linear equations and the cost function is quadratic in terms of the states and inputs.

Assume that the process to be controlled can be described by discrete-time LTI dynamical system, such as the following state-space form:

$$\begin{aligned} x_{t+1} &= Ax_t + Bu_t \\ y_t &= Cx_t \end{aligned} \tag{1.1}$$

where $x_t \in \mathbb{R}^n$ is the actual system state, $u_t \in \mathbb{R}^m$ is the system input and $y_t \in \mathbb{R}^p$ is the measured output, all considered at a certain discrete time instant t. The state at the subsequent time instant $t+1$ is referred to as x_{t+1}.

$A \in \mathbb{R}^{n\times n}$ and $B \in \mathbb{R}^{n\times m}$ are the state and input matrices, respectively. In the context of this thesis is possible to assume the full state information available, thus the input matrix $C \in \mathbb{R}^{p\times n}$ is the identity.

The main goal of the control task is to achieve optimal regulation of the system's states towards the origin. The notion of optimality, in this context, is framed within a quadratic objective function. The LQR problem, therefore, can be viewed as a multi-objective optimization task, where the goal is to simultaneously minimize competing objectives. For example, minimizing the deviation of the system's states from desired values may require higher control effort, and vice versa. In the context of multi-objective optimization, the challenge lies in finding a balance between these conflicting objectives and this always involves making trade-offs to achieve a satisfactory solution.

The Infinite Horizon Linear Quadratic Regulator problem is defined as follows: find the optimal control input u_t, $\forall t \in [0, \infty)$ that makes the following quadratic criteria as small as possible

$$J(\boldsymbol{x}, \boldsymbol{u}) = \sum_{t=0}^{+\infty} x_t^\top Q x_t + u_t^\top R u_t \tag{1.2}$$

where $Q \in \mathbb{R}^{n\times n}$ and $R \in \mathbb{R}^{m\times m}$ are symmetric positive-definite weight matrices.

The vector $\boldsymbol{u}$, also known as input trajectory, consists of the input elements, i.e. $\boldsymbol{u} = \{u_0, u_1, \dots\}$ and $\boldsymbol{x}$, the state trajectory, consists of the states along the infinite time horizon, i.e $\boldsymbol{x} = \{x_1, x_2, \dots\}$. The cost function in (1.2) can be seen as the mathematical formulation of the trade-off between the two objectives to be minimized. Specifically the term $x_t^\top Q x_t$ penalizes deviations of the system's states from desired values, while $u_t^\top R u_t$ penalizes excessive control effort. The weights of the Q and R, typically chosen as diagonal matrices, can be adjusted to find solutions that strike an appropriate balance between minimizing state deviations and control effort.

The overall LQR problem can be mathematically translated into the following optimization problem:

$$\begin{aligned} \min_{\boldsymbol{x},\boldsymbol{u}} \quad & \sum_{t=0}^{+\infty} x_t^\top Q x_t + u_t^\top R u_t \\ \text{subj. to} \quad & x_{t+1} = A x_t + B u_t \qquad\qquad t = 0, 1 \ldots. \\ & x_0 = x_{\text{init}} \end{aligned} \tag{1.3}$$

where $x_{\text{init}} \in \mathbb{R}^n$ is the initial condition of the system at time $t = 0$.

Assuming the pair (A, B) to be controllable and the pair (A, C) with $Q = C^\top C$ to be observable, holds:

- there exists a unique positive definite P_∞ solution of the following equation called Algebraic Riccati Equation (ARE)

$$P_\infty = Q + A^\top P_\infty A - A^\top P_\infty B(R + B^\top P_\infty B)^{-1} B^\top P_\infty A. \tag{1.4}$$

- exploiting the first-order necessary and sufficient conditions for optimality, the optimal control law is a closed form solution, feedback of the state

$$u_t^* = K x_t^* \tag{1.5}$$

with

$$K = -(B^\top P_\infty B + R)^{-1}(B^\top P_\infty A) \tag{1.6}$$

and it is able to asymptotically stabilize the system.

The pair (x_t^*, u_t^*) is the optimal state and input at discrete time instant t.

Despite the fact that one of the main applications of LQ optimal control is regulation, this strategy can be used to track a desired system behaviour as closely as possible, in the framework of Linear Quadratic Tracking (LQT) [14]. To incorporate the desired behaviour to be tracked in the objective, the problem can be written as:

$$\begin{aligned} \min_{\boldsymbol{x},\boldsymbol{u}} \quad & \sum_{t=0}^{+\infty} (x_t - x_{t,\text{des}})^\top Q (x_t - x_{t,\text{des}}) + u_t^\top R u_t \\ \text{subj. to} \quad & x_{t+1} = A x_t + B u_t \qquad\qquad t = 0, 1 \ldots. \\ & x_0 = x_{\text{init}} \end{aligned} \tag{1.7}$$

where $x_{t,\text{des}} \in \mathbb{R}^n$ is the reference state value we want our system's states to track at time t.

Cost function quantifies the controlled system's performance, defined as a weighted sum of the deviations of the system's states from desired values and control effort.

In the context of tracking a given desired state behaviour x_{des} the optimal feedback control law is modified in the following way:

$$u_t^* = K(x_t - x_{t,\text{des}}) \tag{1.8}$$

where the term $x_t - x_{t,\text{des}}$ is the tracking error at time t.

The effectiveness of LQR lies in its ability to leverage the full state information of the system, enabling precise and efficient control.

1.2 Linear Model Predictive Control

Model Predictive Control (MPC) is a modern control strategy renowned for its capacity to provide optimized responses while accounting for state and input constraints, such as saturation limits. These constraints can be explicitly integrated into the control design, enhancing the robustness and performance of the system. The origin of MPC trace back to the mid-seventies to mid-eighties, initially emerging in industrial applications. However, it was not until the nineties that MPC theory underwent significant advancements, leading to its widespread adoption and refinement.

MPC relies on the provided dynamic model to predict the behaviour of the system and determine the optimal control action based on the chosen performance criteria. A key aspect of MPC design is selecting a suitable model, one that adequately describes the system's dynamics while maintaining simplicity to ensure tractability and real-time solvability of the optimization problem.

The description of the linear discrete-time system prediction model is the same shown in (1.1).

For what regards the states and inputs constraints they can be expressed as follows

$$x_t \in \mathcal{X} \qquad \forall t = 0, 1, \dots \tag{1.9}$$

$$u_t \in \mathcal{U} \qquad \forall t = 0, 1, \dots \tag{1.10}$$

the state set $\mathcal{X}$ is closed and the input set $\mathcal{U}$ is compact and non-empty. Usually the sets are described with linear inequalities and both sets are convex and contain the origin.

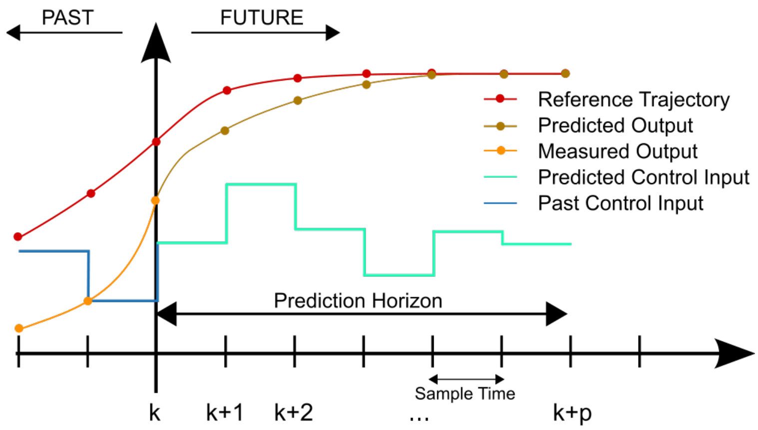

Figure 1.1: Model Predictive Control receiding horizon scheme

Similarly to the LQR case, Model Predictive Control aims to minimize a cost function by defining positive definite matrices Q and R. The goal is to find the optimal control input that minimizes a cost function that takes the following form:

$$J(\boldsymbol{x}, \boldsymbol{u}; x_t, t) = \sum_{i=t}^{+\infty} x_{i|t}^\top Q\, x_{i|t} + u_{i|t}^\top R\, u_{i|t} \tag{1.11}$$

In this formulation $x_{i|t}$ represents the predicted state a time i, given the initial state $x_t = x_{t|t}$. Similarly, $u_{i|t}$ is the predicted control sequence at current time t found considering the entire future predicted trajectory for the system.

The aforementioned formulation represents the infinite horizon MPC problem, that in many practical cases results challenging to be implemented or requires highly demanding computations. For this reason usually MPC formulations optimize only on a finite horizon N, thus the problem of tracking x_{des} with the system's states becomes:

$$\begin{aligned}
\min_{\boldsymbol{x},\boldsymbol{u}} \quad & \sum_{i=t}^{t+N-1} \left(x_{i|t} - x_{t,\text{des}}\right)^\top Q \left(x_{i|t} - x_{t,\text{des}}\right) + u_{i|t}^\top R\, u_{i|t} \\
\text{subj. to} \quad & x_{i+1|t} = A x_{i|t} + B u_{i|t} \qquad\qquad t = 0, 1 \ldots N \\
& x_{i|t} \in \mathcal{X} \\
& u_{i|t} \in \mathcal{U} \\
& x_{t|t} = x_{\text{meas}}(t)
\end{aligned} \tag{1.12}$$

The control law is applied based on the receding horizon principle, which is a key feature of MPC. This principle dictates that at each time instance t, an open-loop optimal control problem is solved using the current state of the plant x_{meas} as the initial state, in order to obtain the control action. All predicted states and inputs within a prediction horizon N are optimized to find an optimal input sequence. However, only the first input of the optimal control sequence generated by the optimization is injected into the plant. This input is used to control the system over the next time step. This procedure is repeated, as illustrated in figure 1.1, at each time instance and by continuously updating the control action based on the most recent information, MPC ensures that the control strategy adapts to changes in the system dynamics and external conditions over time.

1.3 Offset-free tracking MPC and Disturbance Observer

Regulating nonlinear systems using a linear predictive control framework can be a complex task and the model-plant mismatch due to the unmodeled nonlinear dynamics effects, can result in suboptimal performances of the controller.

Even if MPC is able to react to small unmodeled dynamics effects through the receding-horizon fashion, it is not able to consider them inside the predictions, thus to optimize upon them. MPC solves at each time an optimal control problem using the nominal model of the controlled process and, only when the actual plant behaviour closely matches the nominal model, the feedback control scheme can be guaranteed to stabilize the system, and achieve precise tracking of desired setpoints without any offset.

Offset-free Model Predictive Control represents an advanced control strategy designed to address this limitation. It aims to achieve zero steady-state tracking errors in the controlled system, even in presence of disturbances or model uncertainties that cause model-plant mismatch. For instance, in the context of regulating nonlinear systems using a linear predictive control framework, offset-free MPC seeks to regulate the system to its desired setpoint without steady-state error, ensuring precise and accurate control performance.

Consider a discrete-time, time-invariant system describing the plant:

$$\begin{aligned} x_{m,t+1} &= f_m(x_{m,t}, u_t) \\ y_{m,t} &= h_m(x_{m,t}) \end{aligned} \tag{1.13}$$

where $x_{m,t} \in \mathbb{R}^n$, $u_t \in \mathbb{R}^m$ and $y_{m,t} \in \mathbb{R}^p$ are the state, input and plant measured output respectively at time t.

The aim of the offset-free model predictive controller is to have y_m tracking a certain reference signal $y_{\text{des}} \in \mathbb{R}^p$ that is assumed to asymptotically converge to a constant.

Let $w \in \mathbb{R}^n$ and $v \in \mathbb{R}^p$ be defined as:

$$\begin{aligned} w &:= f_m(x_m, u_t) - (Ax + Bu) \\ v &:= h_m(x_m) - Cx \end{aligned} \tag{1.14}$$

where $w \in \mathbb{R}^n$ is the model mismatch between the non-linear plant model and the linear predictive model, $v \in \mathbb{R}^m$ is the output mismatch between predicted output and the real measured plant one. The A, B and C matrices are the ones mentioned in the linear model (1.1).

The key feature of this offset-free control strategy lies in the incorporation of a disturbance model in the prediction model (1.1). This disturbance allows to capture the mismatch between the linear prediction model (1.1) and the nonlinear plant (1.13) in steady state, thus the w term, and to consider it inside the optimization.

The steps that have to be followed, in order to have an offset-free MPC formulation, are the following:

1. Introduce an augmented prediction model with an additional integrating state known as disturbance and modeling the model-plant mismatch
2. Design a state and disturbance estimator based on the augmented model
3. Modify the MPC formulation into an offset-free one considering the estimated disturbance in the formulation

Each point will be properly explained in the following.

Augmented model with disturbance

Accordingly the given introduction, the first step consists in introducing an augmented model for computing the system's predictions in the offset-free MPC framework. It can be, in general, written in the following form:

$$\begin{aligned} x_{t+1} &= Ax_t + Bu_t + B_d d_t \\ d_{t+1} &= d_t \\ y_t &= Cx_t + C_d d_t \end{aligned} \tag{1.15}$$

where the additional state $d_t \in \mathbb{R}^{n_d}$, known as disturbance state or simply disturbance, is assumed to be constant and follows an integral dynamics, as proposed by [15]. The pair (B_d, C_d), where $B_d \in \mathbb{R}^{n \times n_d}$ and $C_d \in \mathbb{R}^{m \times n_d}$, can be seen as the disturbance model matrices. The maximum dimension of the disturbance state has to be equal to the number of measured outputs, i.e. $n_d \leq p$.

Disturbance observer and estimator

Assuming observability of the augmented system (1.15), an estimator that continuously estimates the augmented state (x, d) can be designed. An example could be a linear disturbance observer, that uses the prediction error between the real plant output and the predicted one, to estimate the augmented state as described by the following dynamical system:

$$\begin{aligned}\begin{bmatrix}\hat{x}_{t+1}\\ \hat{d}_{t+1}\end{bmatrix} &= \begin{bmatrix}A & B_d\\ 0 & I\end{bmatrix}\begin{bmatrix}\hat{x}_t\\ \hat{d}_t\end{bmatrix} + \begin{bmatrix}B\\ 0\end{bmatrix}u + \begin{bmatrix}L_x\\ L_d\end{bmatrix}(-y_{m,t} + \begin{bmatrix}C & C_d\end{bmatrix}\begin{bmatrix}\hat{x}_t\\ \hat{d}_t\end{bmatrix})\\ &= A_e\begin{bmatrix}\hat{x}_t\\ \hat{d}_t\end{bmatrix} + B_e\,u + L(-y_{m,t} + C_e\begin{bmatrix}\hat{x}_t\\ \hat{d}_t\end{bmatrix})\end{aligned} \tag{1.16}$$

where $\hat{x} \in \mathbb{R}^n$ and $\hat{d} \in \mathbb{R}^{n_d}$ are the state and disturbance estimates.

The matrices $A_e \in \mathbb{R}^{(n+n_d)\times(n+n_d)}$, $B_e \in \mathbb{R}^{(n+n_d)\times m}$ and $C_e \in \mathbb{R}^{p\times(n+n_d)}$ are the following:

$$A_e = \begin{bmatrix}A & B_d\\ 0 & I\end{bmatrix}, \quad B_e = \begin{bmatrix}B\\ 0\end{bmatrix}, \quad C_e = \begin{bmatrix}C & C_d\end{bmatrix}. \tag{1.17}$$

The $L \in \mathbb{R}^{(n+n_d)\times p}$ matrix is described as follows:

$$L = \begin{bmatrix}L_x\\ L_d\end{bmatrix} \tag{1.18}$$

The system in (1.16) estimates, at each time instant t the unknown disturbance (i.e. the model-plant mismatch in this context) in addition to states. The estimation is performed evaluating the prediction error between the measured plant output and the predicted one.

Offset-free MPC formulation

Given the current estimates of the augmented state $(\hat{x}_t, \hat{d}_t)$ at discrete time t, the MPC classical formulation is modified into an offset-free MPC formulation.

The estimated variables $(\hat{x}_t, \hat{d}_t)$ are used as initial states for the MPC optimization problem at the current solving time instant t. The augmented model in (1.15) is used as prediction model: the disturbance is added both as a constant state, and in the state evolution.

The resulting formulation is the following one:

$$\begin{aligned}
\min_{\boldsymbol{x},\boldsymbol{u}} \quad & \sum_{i=t}^{t+N-1} (x_{i|t} - \bar{x}_t)^\top Q\,(x_{i|t} - \bar{x}_t) + (u_{i|t} - \bar{u}_t)^\top R\,(u_{i|t} - \bar{u}_t) \\
\text{subj. to} \quad & x_{i+1|t} = Ax_{i|t} + Bu_{i|t} + B_d d_{i|t} \qquad\qquad t = 0, 1 \dots N \\
& d_{i+1|t} = d_{i|t} \\
& x_{i|t} \in \mathcal{X} \\
& u_{i|t} \in \mathcal{U} \\
& x_{t|t} = \hat{x}_t \\
& d_{t|t} = \hat{d}_t
\end{aligned} \tag{1.19}$$

where $\bar{x}_t \in \mathbb{R}^n$ and $\bar{u}_t \in \mathbb{R}^m$ are solution of the following system:

$$\begin{bmatrix} A - I & B \\ C & 0 \end{bmatrix} \begin{bmatrix} \bar{x}_t \\ \bar{u}_t \end{bmatrix} = \begin{bmatrix} -B_d \hat{d}_t \\ y_{\text{des}} - C_d \hat{d}_t \end{bmatrix} \tag{1.20}$$

In the last system the coefficient matrix, or left-hand side matrix, represents the dynamics of the system according to the linear model, thus the (A, B, C) matrices. The right-hand side vector, on the contrary, takes into account the disturbance model, thus the (B_d, C_d) matrices, the estimated disturbance $\hat{d}$ and the desired plant reference setpoint y_{des}. This system could be in general overconstrained, meaning there may not exist a solution that satisfies all equations exactly, and the solution is typically found using the least square method with the pseudoinverse.

Luenberger observer design

In this offset-free MPC formulation the nominal augmented state (x, d) needs to be estimated at each time instant, given the plant output measurement y_m, according to the dynamical estimator system in (1.16).

The $L_x \in \mathbb{R}^{n \times p}$ and $L_d \in \mathbb{R}^{n_d \times p}$ observer gain matrices in (1.16) has to be designed in such a way the estimator to be stable, while the method doesn't matter for our purposes.

Two possible choices of state estimator could be Luenberger observer or the Kalman filter. Specifically in the context of this thesis the Luenberger observer has been used. It updates the state prediction computed at time $t-1$ using the current measured plant output y_m at time t as in the following:

$$\hat{x}_t = A\hat{x}_{t-1} + Bu_{t-1} + L(y_{m,t} - \hat{y}_t) \tag{1.21}$$

where $\hat{y}_t := C(A\hat{x}_{t-1} + Bu_{t-1})$. The difference $(y_{m,t} - \hat{y}_t)$ is called estimation error or correction term and $L \in \mathbb{R}^{n \times p}$ is the observer gain.

If the pair (A_e, C_e) in (1.16) is observable, than the eigenvalues of $(A_e + LC_e)$ can be placed arbitrarily in such a way the estimator dynamical system to be stable. Usually we want the estimator to be faster with respect to the controller, for this reason the desired eigenvalues for $(A_e + LC_e)$, thus the poles of the estimator dynamical systems, are chosen smaller with respect to the ones of the controlled stabilized system.

Chapter 2

Design of Optimization-based Controller for autonomous airshield

This chapter will provide first of all a description of the go-kart plant model and of its linear approximation used to design the predictive controllers.

Later on a proper description of the design choices and the formulations of both the controllers in the context of the sport application: the Linear Quadratic Regulator (LQR) and the Model Predictive Control (MPC), nominal and with Offset-free version.

2.1 Go-kart kynematics model

The non linear model used to describe the kart dynamics is a bicycle model. 2D bicycle model can be seen as a simplified vehicle model that approximates very well the motion of a 4-wheel vehicle in normal driving conditions.

The mathematical equations are the following:

$$\begin{cases} \dot{x}(t) = v(t)\cos(\psi(t) + \beta(t)) \\ \dot{y}(t) = v(t)\sin(\psi(t) + \beta(t)) \\ \dot{\psi}(t) = \dfrac{v(t)}{l_r}\sin(\beta(t)) \\ \dot{v}(t) = \dfrac{F_x(t)}{m} \end{cases} \tag{2.1}$$

where $x = [x, y, \psi, v]$ is the state vector where the components are respectively the x and y world frame coordinates, ψ the heading angle with respect to the

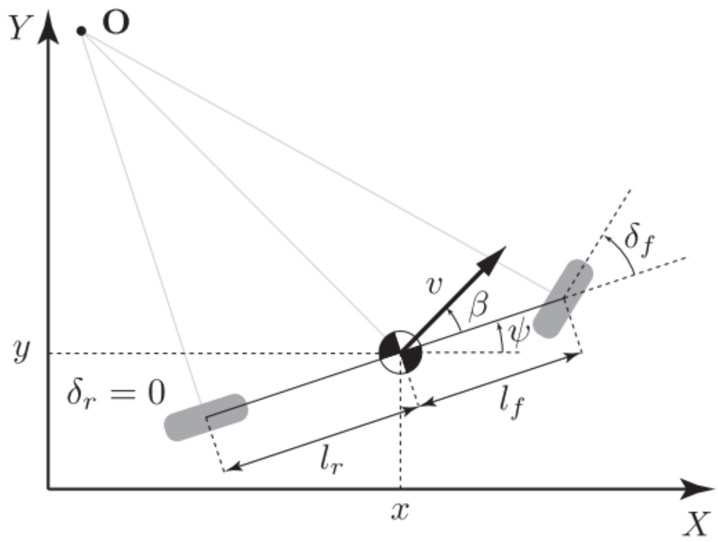

reference frame, and v the total speed of the vehicle.

The longitudinal force F_x acting on the vehicle is modeled as a single force applied to the center of gravity of the vehicle and is computed as a combination of the drive-train command and the velocity.

$$F_x(t) = (C_{m_1} - C_{m_2}v(t))a(t) - C_f v(t) - C_d v^2(t) - C_{roll} \tag{2.2}$$

$$\beta(t) = \arctan\left(\tan\left(\frac{l_r}{l_f + l_r}\delta_f(t)\right)\right). \tag{2.3}$$

The inputs of this system are $u = [a, \delta_f]$ where a is the drive-train acceleration and δ_f the front steering angle. The variable β is the slip angle at the center of mass.

The model has two parameters, l_f and l_r, which represent the distances from the centre of mass to the front axle and rear axle, respectively.

The mass $m = 300$ Kg includes both the kart and the trailer weight, while $l_f = l_r = 0.8$ meters. The other parameters of this model have been identified as reported in table 2.1.

The identified coefficients represent:

- C_{roll} : rolling coefficient modeling the wheel friction on the road surface
- C_d : coefficient modeling aerodynamic resistance or drag
- C_f : coefficient modeling the dynamic friction resistance
- C_{m1} : coefficient associated with the force component due to the driving torque of the vehicle

- C_{m2} : coefficient associated with the force component due to both the torque and the velocity

C_{m1}	930
C_{m2}	0
C_f	10
C_d	1.5
C_{roll}	73

Table 2.1: Identified parameters for bicycle model

According to the estimated values the (2.2) can be rewritten as follows:

$$F_x(t) = C_{m1}a(t) - C_f v(t) - C_d v^2(t) - Croll \tag{2.4}$$

The physical actuations limits on the input variable a can be expressed as box constraints of the following type:

$$a_{\min} \leq a_t \leq a_{\max} \tag{2.5}$$

The coefficients reported in table 2.1 are identified in such a way to have $a_{min} = 0$ and $a_{max} = 1$ as actuation limits for the motor torque.

2.2 Linear approximation of the system dynamics

The system is specifically designed for overspeed training of Olympic runners. For this kind of high energetic demanding training, the athletes are interested in executing only short distances of approximately $50 - 60$ meters performed on the straightway of the track and field oval-shaped racetrack. For this reason it is reasonable to consider only the longitudinal motion of the vehicle along one direction and not taking anymore into account the steering degree of freedom. Additionally, the go-kart is designed such that an onboard driver must be present for safety reasons and to control the steering when maneuvering the go-kart back to the starting line of the sprint.

According this assumption rectlinear motion assumption, the go-kart plant model in (2.1) can be simplified as in the following:

$$\begin{cases} \dot{p}(t) = v(t) \\ \dot{v}(t) = \dfrac{F_x(t)}{m} = \dfrac{1}{m}(C_{m1}a(t) - C_f v(t) - C_d v^2(t) - C_{roll}) \end{cases} \tag{2.6}$$

where p indicates the position of the vehicle along an arbitrarily oriented direction.

Examining the equations, it can be noticed that a good linear approximation of (2.6) can be found and used for the longitudinal controller design. The only non linear term is in fact the one related to the drag coefficient in the equation describing the longitudinal force. Assuming that in the context of this application, the velocities the kart exploits during the motion are quite small, this term will be small as well.

Accordingly, continuous time dynamics equations of the linear approximation model can be obtained by just removing that non linear term:

$$\begin{cases} \dot{p}(t) = v(t) \\ \dot{v}(t) = \dfrac{F(t)}{m} = \dfrac{1}{m}(C_{m1}a(t) - C_f v(t)) \end{cases} \tag{2.7}$$

The Forward Euler method is used for discretize the given continuous-time dynamical system:

$$y_{t+1} = y_t + dt \cdot f(y_t, t) \tag{2.8}$$

where f is the continuous time function and dt is the discrete-time step size, distance between two consecutive discretization steps.

It is possible to write the following linear discrete-time, time-invariant system:

$$\begin{cases} p_{k,t+1} = p_{k,t} + dt\, v_{k,t} \\ v_{k,t+1} = v_{k,t} + dt\left(\dfrac{C_{m1}}{m}u_t - \dfrac{C_f}{m}v_{k,t}\right) \end{cases} \tag{2.9}$$

And moving into the state space form it can be rewritten as:

$$\begin{aligned} x_{k,t+1} = \begin{bmatrix} p_{k,t+1} \\ v_{k,t+1} \end{bmatrix} &= \begin{bmatrix} 1 & dt \\ 0 & 1 - dt\frac{C_f}{m} \end{bmatrix} x_{k,t} + \begin{bmatrix} 0 \\ dt\frac{C_{m1}}{m} \end{bmatrix} u_t \\ &= A\, x_{k,t} + B\, u_t \end{aligned} \tag{2.10}$$

where $x_k = [p_k, v_k]^\top$ are the kart state variables expressing respectively the kart position and the kart velocity and $u = a$ is the control input of the system, while dt is the sampling step used for Euler forward integration.

This linear model is the one used as basic for the controllers design in the following.

2.3 Gain Scheduling LQR design

Consider that at each time instant the information about the runner state $x_r = [p_r, v_r]^T$ is known, where p_r represents the absolute runner position and v_r indicates the absolute runner velocity.

At each time instant t the desired state for the go-kart is given by:

$$x_{k,\text{des}} = \begin{bmatrix} p_r + d_{\text{des}} \\ v_r \end{bmatrix} \tag{2.11}$$

where d_{des} denotes the reference distance between the kart and the runner. Using this reference, the closed-form control law in 1.8 is applied to obtain the optimal unconstrained solution u^* , at each time instant.

While MPC explicitly incorporates constraints into the optimization problem, LQR does not provide a direct mechanism for handling constraints. Constraints can be indirectly addressed by penalizing their violation in the cost function, but it's still possible to deal with control actions that violate certain physical limits, such as those described in 2.5. To address this, the unconstrained control actions generated by the LQR controller has been "clipped" as follows:

$$\tilde{u}^* = \text{sat}_{[a_{min}, a_{max}]}(u^*) \tag{2.12}$$

The value $\tilde{u}^*$ can be referred to as the clipped-unconstrained optimal LQR control action. While clipping allows the controller to handle constraints in a straightforward manner, it can lead to suboptimal performances, as the controller may be forced to operate at the constraint boundaries. Therefore, alternative approaches such as MPC may be preferred for systems with stringent constraint requirements.

From the control architecture point of view a gain scheduling approach has been introduced in the control scheme. A gain scheduling controller is a type of control design that allows to dynamically switch between different control laws or gains based on certain operating conditions or parameters. In the context of this thesis one among two difference LQR controllers is selected and used to regulate the system to the desired reference value. They will be explained in details in the following.

2.3.1 Catch-up maneuver

The most challenging phase of the motion occurs in the first few seconds when the runner accelerates faster than the maximum acceleration the kart can achieve. This

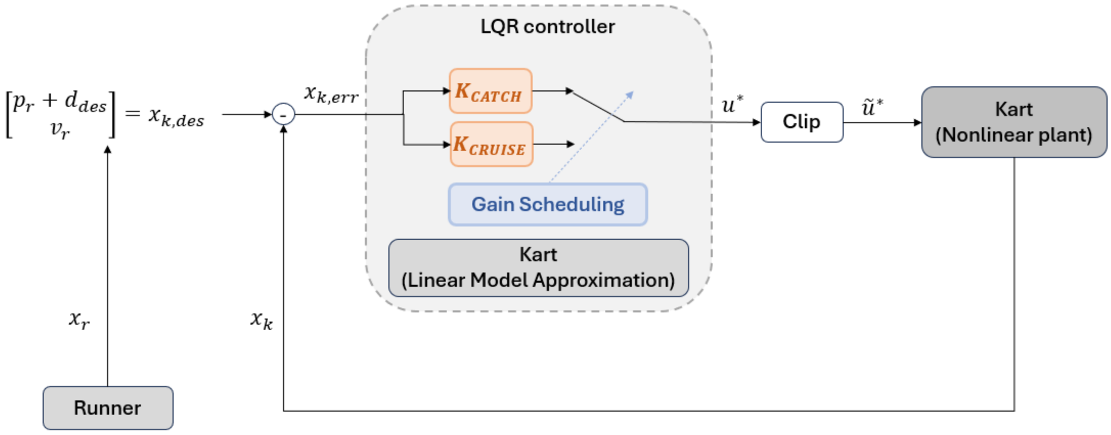

Figure 2.1: Linear Quadratic Regulator control scheme

phase is referred to as the 'catch-up maneuver'. To prevent a potential collision between the airshield and the runner, a safety measure is implemented, requiring the runner to begin the sprint performance from a position several meters farther from the kart, with respect to the steady state desired distance d_{des}.

Hence, the initial condition for the kart state is set to be the following:

$$x_{k,\text{init}} = \begin{bmatrix} d_{\text{des}} + \bar{d} \\ 0 \end{bmatrix} \tag{2.13}$$

where $\bar{d}$ is a parameter that depends on how fast the runner is going to accelerate during his performance.

During the catch-up phase, the control action is governed by the controller gain K_{catch} computed using the following weights:

$$Q_{\text{catch}} = \begin{bmatrix} 40 & 0 \\ 0 & 1000 \end{bmatrix}, \quad R_{\text{catch}} = [2] \tag{2.14}$$

As evidenced by the weight selection, during the catch-up maneuver, the primary objective during the catch-up maneuver is to match the go-kart velocity with that of the runner. For this reason a significantly higher weight is assigned to the second state variable. This weights configuration enables the kart to start accelerating at its maximum capability, even if the runner remains at a distance greater than the desired value d_{des}. Such an approach serves to avoid an unsafe scenarios, particularly situations where the runner's higher velocity could lead to a collision with the shield.

2.3.2 Cruise maneuver

Once the alignement between the kart and runner velocity is achieved, typically at an 80% match, the controller switches to K_{cruise} which assigns nearly equal importance to distance and velocity mismatch. While a preference for the velocity state persists, the significance given to the kart's position relative to the runner's is significantly increased.

The weight matrices for this cruise control configuration are as follows:

$$Q_{\text{cruise}} = \begin{bmatrix} 800 & 0 \\ 0 & 4000 \end{bmatrix}, \quad R_{\text{cruise}} = [0.002] \tag{2.15}$$

This setup enables a rapid and substantial reduction in the relative distance to the desired value once the velocities of the go-kart and runner closely align. Once the desired value d_{des} is reached, the K_{cruise} controller and its corresponding control law maintain the system around the desired operating conditions.

The overall control scheme is the one shown in figure 2.1, while algorithm 1 outlines the steps followed by the LQR algorithm while controlling the system.

Algorithm 1 LQR implementation

catched = false;
Set initial runner position with a proper distance $\bar{d}$ from kart;
for $t = 0, 1, 2, ...$ **do**;
    Take kart state information $x_{k,t} = [p_{k,t}, v_{k,t}]^\top$;
    Take runner state information $x_{r,t} = [p_{r,t}, v_{r,t}]^\top$;
    Compute corresponding desired state for kart $x_{k,t,des} = [p_{r,t} + d_{\text{des}}, v_{r,t}]^\top$;
    if $v_{k,t} \geq 0.8 v_{r,t}$ **and** catched = false **then**
        catched = true;
    end if
    if catched = false **then**
        $u^* = -K_{\text{catch}}(x_{k,t} - x_{k,t,des})$;
    else
        $u^* = -K_{\text{cruise}}(x_{k,t} - x_{k,t,des})$;
    end if
    Clip input according to limit saturation limits $\tilde{u}^* = \text{sat}_{[a_{\min}, a_{\max}]}(u^*)$;
    Inject $\tilde{u}^*$ in the plant;
end for

2.4 MPC design

The main purpose of the Model Predictive Control scheme design lies in the possibility of including constraints, in the incorporation of a runner model inside the prediction one and in the simplification of the overall control scheme. The gain scheduling approach switching between two controllers depending on the operation conditions can be replaced with a single MPC controller. Explicitly including constraints in the MPC formulation enables the encoding of safety guarantees within the control scheme. Examples of such constraints include maintaining a minimum safety distance or imposing bounds on maximum velocities to mitigate the risk of injuries.

Consider the linear model approximation 2.10 for the go-kart dynamics, and introduce the following integrator model for the runner, considered as an autonomous system:

$$\begin{cases} p_{r,t+1} = p_{r,t} + dt\, v_{r,t} \\ v_{r,t+1} = v_{r,t} + dt\, a_{r,t} \end{cases} \tag{2.16}$$

This model assumes constant acceleration for the runner, providing a simplified yet effective representation of their behavior.

Incorporating this assumption, we define the augmented state for the MPC prediction model as:

$$x_p = \begin{bmatrix} \Delta p \\ \Delta v \\ v_k \end{bmatrix} \tag{2.17}$$

where $\Delta p := p_k - p_r$ and $\Delta v := v_k - v_r$ represent the relative distance and velocity between the kart and the runner at a given time, respectively.

The overall prediction model, in discrete-time, state-space formulation can be written as follows:

$$\begin{aligned} x_{p,t+1} = \begin{bmatrix} \Delta p_{t+1} \\ \Delta v_{t+1} \\ v_{k,t+1} \end{bmatrix} &= \begin{bmatrix} 1 & dt & 0 \\ 0 & 1 & -dt\frac{C_f}{m} \\ 0 & 0 & 1 - dt\frac{C_f}{m} \end{bmatrix} x_{p,t} + \begin{bmatrix} 0 \\ dt\frac{C_{m1}}{m} \\ dt\frac{C_{m1}}{m} \end{bmatrix} u_t + \begin{bmatrix} 0 \\ -dt a_{r,t} \\ 0 \end{bmatrix} \\ &= A_p\, x_{p,t} + B_p\, u_t + a_t \end{aligned} \tag{2.18}$$

where

$$A_p = \begin{bmatrix} 1 & dt & 0 \\ 0 & 1 & -dt\frac{C_f}{m} \\ 0 & 0 & 1 - dt\frac{C_f}{m} \end{bmatrix} \quad B_e = \begin{bmatrix} 0 \\ dt\frac{C_{m1}}{m} \\ dt\frac{C_{m1}}{m} \end{bmatrix}. \tag{2.19}$$

The runner actual acceleration $a_{r,t}$ is considered to be known and introduced in the prediction model as a linear affine term that allows the predictions to better fit with the real future runner behaviour. This term relative to the actual runner acceleration can be seen as the introduction of a known disturbance in the system, thus $a_t = [0, -dt a_{r,t}, 0]^\top$.

The optimal control problem solved at each discrete time instant, in a receiding horizon fashion, has the following formulation:

$$\begin{aligned} \min_{\boldsymbol{x},\boldsymbol{u}} \quad & \sum_{i=t}^{t+N-1} (x_{p,i|t} - x_{p,\text{des}})^\top Q\, (x_{p,i|t} - x_{p,\text{des}}) + u_{i|t}^\top R\, u_{i|t} \\ \text{subj. to} \quad & x_{p,i+1|t} = A_p\, x_{p,i|t} + B_p\, u_{i|t} + a_t \qquad\qquad t = 0, 1 \ldots N \\ & a_{\min} \leq u_{i|t} \leq a_{\max} \\ & d_{\text{safe}} \leq \Delta p_{i|t} \\ & x_{p,t|t} = x_{p,\text{meas}} \end{aligned} \tag{2.20}$$

where the reference values for the prediction states are the following

$$x_{p,\text{des}} = \begin{bmatrix} d_{\text{des}} \\ 0 \\ 0 \end{bmatrix} \tag{2.21}$$

and d_{safe} is a minimum distance between go-kart and runner, ensuring a safe situation.

The parameter N defines the prediction horizon thus the number of control intervals the controller must evaluate by prediction. This parameter must be carefully selected since the complexity of solving the optimization problem increases when the prediction horizon increases. This problem could have important consequences in systems having fast dynamics, where the number of prediction steps is limited by the processor power. At the same time the prediction horizon has to be chosen long enought to adequately capture the system dynamics. The optimal input sequence, found by repeatedly solving at each time step the optimizaton problem, is such that $\boldsymbol{u}^* \in \mathbb{R}^{m \times N}$.

The weights in the cost function are much less sensible to changes with respect to the ones used in the LQR formulation and are chosen like:

$$Q = \begin{bmatrix} 2.5 & 0 & 0 \\ 0 & 5 & 0 \\ 0 & 0 & 0 \end{bmatrix}, \quad R = [0.02] \tag{2.22}$$

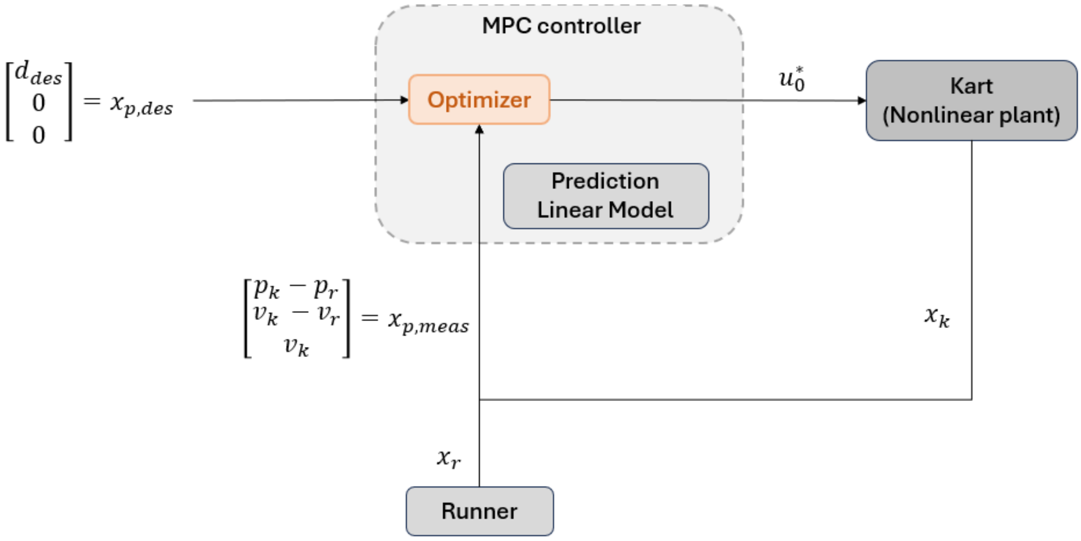

Figure 2.2: Model Predictive Control scheme

The last element in the Q matrix is chosen to be equal to zero since a reference for the absolute kart velocity is not present. For this reason the third state is not taken into account in the cost function of the optimization problem but it is kept in the state vector because it makes possible to write the prediction model in an easier way.

Algorithm 2 MPC implementation

1: Define desired prediction state $x_{p,\text{des}} = [d_{\text{des}}, 0, 0]^\top$;
2: Set initial runner position with a proper distance $\bar{d}$ from kart;
3: **for** $t = 0, 1, 2, \ldots$ **do**
4: Take prediction state information $x_{p,t} = [\Delta p_t, \Delta v_t, v_{k,t}]^\top$;
5: Solve the constrained QP and get $\boldsymbol{u}^* = \{u_0, u_1, \cdots, u_N\}$;
6: Inject the first element of the optimal input sequence u_0^* in the plant;
7: **end for**

The overall MPC control scheme is shown in 2.2. It is easy to understand the semplification in the architecture achieved with the MPC, with respect to the LQR case shown in 2.1. Algorithm 2 describes the points of the MPC implementation.

2.5 Offset-free MPC and disturbance observer design

The MPC problem formulated in (2.20) employs as prediction model a linear approximation of the kart dynamics (see (2.10)), augmented with the runner model in (2.16). However, this prediction model does not take into account the nonlinear term arising from the drag coefficient present in the identified kart dynamic equations in 2.6. In particular the true nonlinear prediction model for the MPC should result in the following formulation:

$$\begin{bmatrix} \Delta p_{t+1} \\ \Delta v_{t+1} \\ v_{k,t+1} \end{bmatrix} = \begin{bmatrix} 1 & dt & 0 \\ 0 & 1 & -dt\frac{C_f}{m} \\ 0 & 0 & 1-dt\frac{C_f}{m} \end{bmatrix} x_{p,t} + \begin{bmatrix} 0 \\ dt\frac{C_{m1}}{m} \\ dt\frac{C_{m1}}{m} \end{bmatrix} u_t + \begin{bmatrix} 0 \\ -dt a_{r,t} \\ 0 \end{bmatrix} - \begin{bmatrix} 0 \\ dt(\frac{C_d}{m}v_{k,t}^2 + \frac{C_{roll}}{m}) \\ dt(\frac{C_d}{m}v_{k,t}^2 + \frac{C_{roll}}{m}) \end{bmatrix} \tag{2.23}$$

where the last term includes the nonlinear, unmodelled drag effect, thus the w term in (1.14) representing the model-plant mismatch term within the offset-free MPC context.

Since MPC derives its solution based on the linear model in (2.18), the performance of the controller are inherently tied to the magnitude of the unmodeled effects. Consequently, optimal closed-loop performance may not be achievable using the nominal MPC formulation. Offset-free MPC is designed to handle this kind of situations where there are discrepancies between the nominal model used for prediction and the actual plant dynamics.

Data-driven control strategies, on the contrary, do not require models and can implicitly manage uncertainties in processes. However, pure data-driven approaches, without any prior assumptions about process necessitate extensive data and typically employ slow exploratory techniques. Recent control methodologies blend model-based techniques with data-driven approaches to overcome these limitations. The reasoning used in this thesis to compensate for the model-plant mismatch term, combines a predictive control based on the linear prediction model, with a real-time estimation and compensation of the nonlinear term based on data from the system. This control strategy dynamically estimates for this discrepancy using the prediction errors, thus the difference between the model's predictions and the actual system response.

Although offset-free MPC can mitigate model-plant mismatch, estimating real-time the disturbance from measurement errors, the observer introduces a delay. This delay has as a consequence the fact that the disturbance compensation may only be optimal at steady-state and not during transient when the disturbance varies.

Considering the problem statement presented in (2.27), the affine term that takes into account the runner acceleration, has been added, similar to the nominal MPC case.

The augmented prediction model in 1.15 necessary to the offset-free formulation is applied and it results to be:

$$\begin{aligned} x_{p,t+1} &= A_p\, x_{p,t} + B_p\, u_t + a_t + B_d\, d_t \\ d_{t+1} &= d_t \end{aligned} \tag{2.24}$$

where the matrices A_p, B_p and the vector a_t are defined in (2.19) and d_t is a scalar.

The term $B_d = [0, 1, 1]^\top$ signifies that the disturbance affects only in the second and third states, while the relative position prediction model remains unaffected by the mismatch with the plant. For the purposes of this thesis the state is considered to be fully observable (i.e. $C = I_3$) and, as a consequence, the reference for the measured plant output is translated in reference for the plant states, thus $y_{\text{des}} = x_{p,\text{des}} = [d_{\text{des}}, 0, 0]^\top$. Accordingly also $C_d = [0, 0, 0]^\top$.

The design of the observer plays a crucial role in enhancing the robustness of the proposed control scheme and it becomes:

$$\begin{bmatrix} \hat{x}_{p,t+1} \\ \hat{d}_{t+1} \end{bmatrix} = A_e \begin{bmatrix} \hat{x}_{p,t} \\ \hat{d}_t \end{bmatrix} + B_e\, u + L(-x_{p,t} + C_e \begin{bmatrix} \hat{x}_{p,t} \\ \hat{d}_t \end{bmatrix}) \tag{2.25}$$

where

$$A_e = \begin{bmatrix} A_p & B_d \\ 0 & 1 \end{bmatrix}, \quad B_e = \begin{bmatrix} B_p \\ 0 \end{bmatrix}, \quad C_e = \begin{bmatrix} I_3 & 0 \end{bmatrix}. \tag{2.26}$$

The observer gain matrix L is designed in such a way the poles of $(A_e + LC_e)$ are placed in $\lambda = [0.5, 0.51, 0.52, 0.53]$, ensuring the resultant matrix to be Hurwitz. The same weighting matrices Q and R utilized in the nominal MPC context are employed as weights.

The final resulting offset-free formulation can be summarized in the following

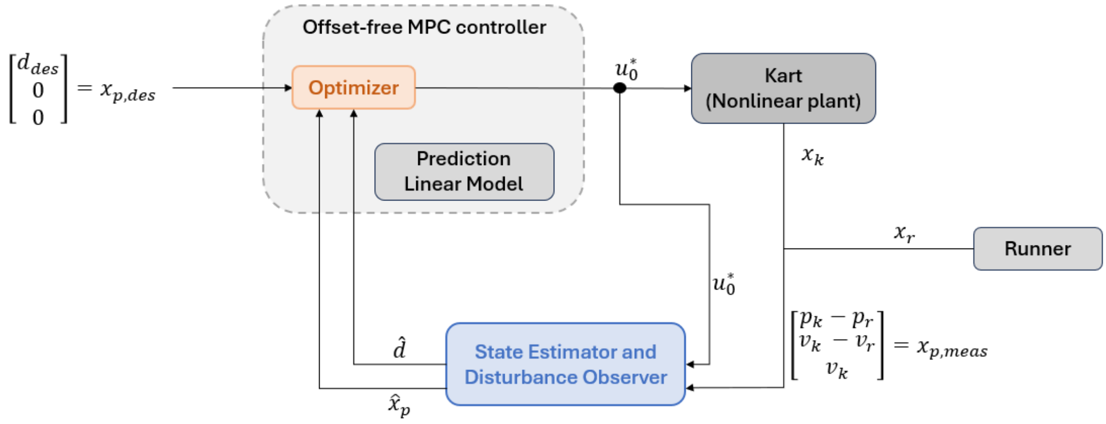

Figure 2.3: Offset-free Model Predictive Control scheme with disturbance observer

constrained optimization problem:

$$\begin{aligned}
\min_{\boldsymbol{x},\boldsymbol{u}} \quad & \sum_{i=t}^{t+N-1} (x_{p,i|t} - \bar{x}_t)^\top Q\,(x_{p,i|t} - \bar{x}_t) + (u_{i|t} - \bar{u}_t)^\top R\,(u_{i|t} - \bar{u}_t) \\
\text{subj. to} \quad & x_{p,i+1|t} = A_e\, x_{p,i|t} + B_e\, u_{i|t} + B_d\, d_{i|t} \qquad\qquad t = 0, 1 \ldots N \\
& d_{i+1|t} = d_{i|t} \\
& a_{\min} \le u_{i|t} \le a_{\max} \\
& d_{\text{safe}} \le \Delta p_{i|t} \\
& x_{p,t|t} = \hat{x}_t \\
& d_{t|t} = \hat{d}_t
\end{aligned} \tag{2.27}$$

where $\bar{x}_t \in \mathbb{R}^n$ and $\bar{u}_t \in \mathbb{R}^m$ are solution of the following system:

$$\begin{bmatrix} A_p - I_3 & B_p \\ I_3 & 0 \end{bmatrix} \begin{bmatrix} \bar{x}_t \\ \bar{u}_t \end{bmatrix} = \begin{bmatrix} -B_d \hat{d}_t \\ x_{p,\text{des}} - C_d \hat{d}_t \end{bmatrix} \tag{2.28}$$

In image 2.3 the block diagram of the proposed offset-free MPC with disturbance observer implementation is represented and algorithm 3 describes the point of both estimation and control followed by the scheme.

Algorithm 3 MPC Offset-free implementation

1: Define desired prediction state $x_{p,\text{des}} = [d_{\text{des}}, 0, 0]^\top$;
2: Set initial runner position with a proper distance $\bar{d}$ from kart;
3: Initialize estimator $\hat{x}_{p,0} = [d_{\text{des}}, 0, 0]^\top$ and $\hat{d}_0 = 0$;
4: **for** $t = 0, 1, 2, ...$ **do**
5: Take state estimator and disturbance observer information $\hat{x}_{p,t}$ and $\hat{d}_t$;
6: Solve the constrained QP and get $\boldsymbol{u}^* = \{u_0, u_1, \cdots, u_N\}$;
7: Inject the first element of the optimal input sequence u_0^* in the plant;
8: Update state estimator and disturbance observer
9: **end for**

2.6 Fluid-dynamic studies

Fluid dynamics is a branch of physics that deals with the study of how fluids (liquids and gases) behave when they are in motion. In the context of sports engineering, fluid dynamics plays a crucial role in understanding the interaction between athletes and the surrounding air or water during their performance.

Aerodynamics, a subfield of fluid dynamics, specifically focuses on the study of how moving objects interact with the air. Drag force, a key parameter in aerodynamics, quantifies the resistance encountered by an object as it moves through a fluid medium. It can be expressed mathematically using the drag equation:

$$F_d = \frac{1}{2} C_d \rho A \, v^2 \tag{2.29}$$

where F_d is the drag force, ρ is the density of fluid (air in this case), A is the frontal area of the object moving in the fluid, v is the velocity of the object ad C_d the drag coefficient. One notable characteristic of drag force is its dependence on the square of the velocity (v^2), indicating that the resistance experienced by an object increases exponentially with its speed.

Recent fluid-dynamic studies and simulations, conducted using wind tunnels and advanced computational methods by [4] has shown the effect of the aerodynamic shield on the variation of the aerodynamic force acting on a runner for a range of speeds between 5 and 13 meters per second.

As depicted in figure 2.4, when the air moving over the shield fails in following the curvature of a surface, it is reparated into two different flows. This leads to the formation of vortices and regions of recirculating flow, creating a large low-pressure region behind the shield. Interestingly, this aerodynamic configuration not

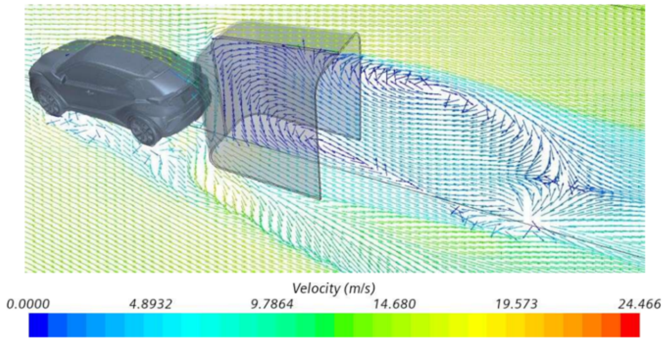

Figure 2.4

only reduces air friction experienced by the athlete but also generates a pushing force from behind, aligning with the athlete's movement. Consequently, the athlete benefits from reduced air resistance and a propulsive force, potentially enhancing their speed and performance.

For this reason the reference distance d_{des} to be kept between the runner and the kart can be assumed to be around 2.5 meters, thus the athlete should be able to run on the airshield border or in the slipstream up to a couple of meters further. In the following, for both the simulations and the real hardware test it is used d_{des} of 2.5 meters and d_{safe} of 1.5 meters.

Chapter 3

Numerical simulation results

The first purpose of this chapter is to present and analyze the results of Python simulations carried out on the non linear mathematical model of the go-kart with the airshield attached, trying to follow a velocity profile simulating the runner behaviour during a competition or a training. The three controllers: Linear Quadratic Regulator, Model Predictive Control and Offset-Free Model Predictive Control have been tested and their performances are evaluated and compared. Specifically in section 3.1, the data utilized for the controllers simulation tests are introduced. Additionally, it is described how they have been obtained from real competition results, together with a presentation of the parameters used for the comparison. Section 3.2 and 3.3 are focused on finally evaluate and numerically compare the controllers performances in two distinct scenario.

3.1 Test data and comparison parameters

To assess the performance of the controllers and evaluate the application's behaviour, empirical data from two presigious Diamond League competitions [16] have been employed, focusing on the winners of the 100m sprint event both in the man's and women's categories.

	10m	20m	30m	40m	50m	60m	70m	80m	90m	100m
t	1.97	3.10	4.11	5.08	6.03	6.99	7.94	8.90	9.88	10.88
Δt	1.97	1.13	1.01	0.97	0.95	0.96	0.95	0.96	0.98	1.00
$\bar{v}_r$	5.07	8.85	9.90	10.31	10.53	10.42	10.53	10.42	10.20	10.00

Table 3.1: Marie-Josèe Ta-Lou - Diamong League Lausanne 30th June 2023

In the case of the women's 100m sprint event, data are taken from the competition held in Lausanne on June 30, 2023. The race saw Marie-Josèe Ta Lous as winner and in table 3.1 are reported her timed intervals recorded at every 10 meters. Based on these splits an average velocity for each 10 meters interval has been computed in order to have a velocity runner profile over time.

	10m	20m	30m	40m	50m	60m	70m	80m	90m	100m
t	1.87	2.89	3.80	4.67	5.52	6.36	7.21	8.07	8.93	9.83
Δt	1.87	1.02	0.91	0.87	0.85	0.84	0.85	0.86	0.86	0.90
$\bar{v}_r$	5.35	9.80	10.99	11.49	11.76	11.90	11.76	11.63	11.63	11.11

Table 3.2: Christian Coleman - Diamong League Eugene 16th September 2023

Likewise, a similar methodology have been applied to the men's 100m competition, which took place in Eugen on September 16, 2023. Christian Coleman clinched victory crossing the finish line in 9.83 seconds. The detailed analysis of Coleman's performance and the corresponding average velocities derived from the intervals times are reported in table 3.2.

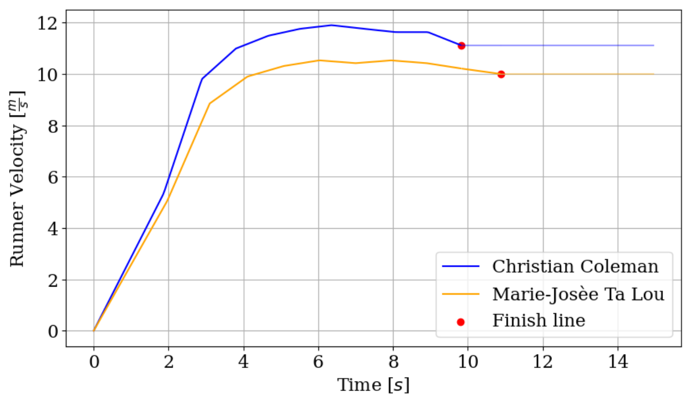

Figure 3.1: Velocities profiles used for simulation tests

The velocity profiles obtained by interpolating the average velocities are illustrated in figure 3.1. The red dot denotes the moment when runners cross the finish line. Subsequent to this event, the velocities are assumed to remain constant until a simulation time of 15 seconds with the purpose of allowing for an evaluation of the controllers' steady-state performance.

The parameters used for the evaluation and comparison of the controllers performances are the following:

- Mean error (position and velocity): represents the average difference between the desired reference value and the actual plant output over the simulation period. It provides a measure of the overall accuracy of the controller's tracking performance.

- Integral Asbolute Error (position and velocity): measured the cumulative sum of the absolute errors between the desired reference value and the actual plant output. It provides insight into the total deviation od the system's response from the desired trajectory.

- Minimum distance from kart: the concept is similar to the undershoot, thus the extent to which the system's response deviates from the desired trajectory. This parameter quantifies how close the runner goes to the kart during the performance.

- Energy consumption: quantifies the amount of energy expended by the controller to achieve the desired tracking performance.

- Stead-state error: characterized the residual errror between the actual output and the desired reference value once the system has reached a stable operating condition, thus a constant velocity of the kart tracking a constant velocity of the runner.

- "Rise" time to reach the desired reference distance d_{des}: refers to the duration taken by the system's output to transition from the initial state to the desired position setpoint. It represents the speed at which the system responds to changes in the reference signal and it's indicative of the controller's dynamic responsiveness.

CVXPY and OSQP solver

The quadratic optimization problems in the MPC formulations have been solved using the CVXPY library [17], mathematical framework used to solve optimization problems and the OSQP solver [18]. CVXPY allows to express the convex optimization problem to be solved according to a natural syntax that follows the math, and is later automatically converted into the standard form required by generic solvers. OSQP (Operator Splitting Quadratic Program) is a high-performance solver for convex quadratic programming problems well suited for applications in control systems, robotics and machine learning.

3.2 Test on women velocity profile of Ta Lou

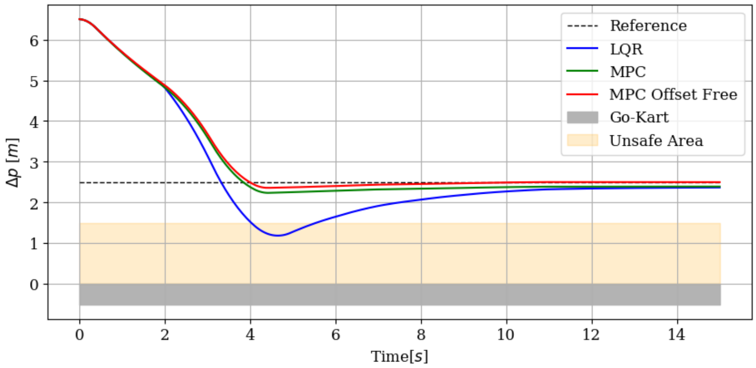

(a) Relative position between runner and go-kart

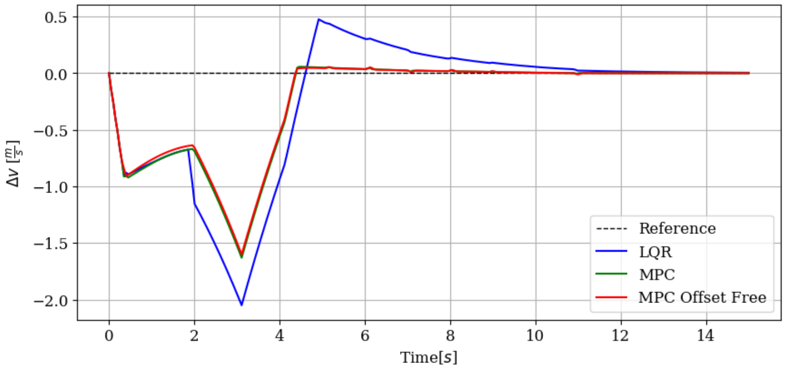

(b) Relative velocity between runner and go-kart

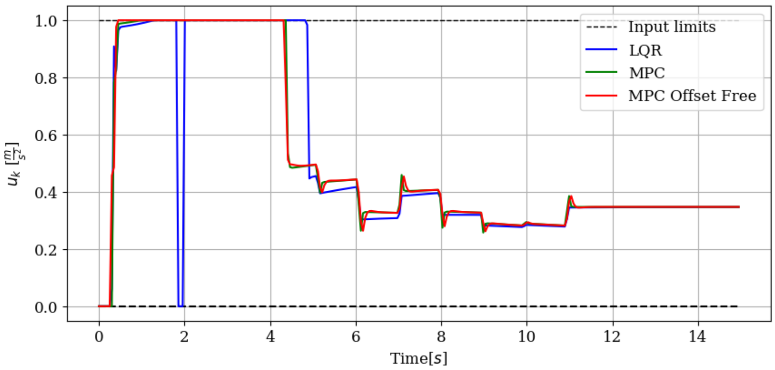

(c) Input effort (drive-train acceleration)

Figure 3.2: Simulation results following Ta Lou velocity profile. The results for LQR (in blue), MPC (in green) and Offset-free MPC (in red) are shown overlapped on the same plot to appreciate the comparison among controllers

The initial distance used for the simulation is $\bar{d} = 4$ meters.

Both Table 3.3 and figure 3.2 clearly demonstrate that the LQR controller exibits poorer performance compared to the other controllers. Specifically, considering the minimum distance between runner and go-kart, the LQR performs significantly worse than the other two controllers and violates the safety distance state constraints d_{safe} introduced in both the MPC formulations. The LQR also has the highest mean value of position deviation (Δp) and velocity deviation (Δv) indicating a less accurate tracking performance compared to MPC and MPC Offset-free. Additionally, the fact that also the Integral of Absolute Error (IAE) metrics for both position and velocity are higher, suggests poorer tracking accuracy over the entire simulation period. It's noteworthy that the offset-free version of the predictive controller achieves an almost zero steady-state error, significantly smaller than the approximately 10-centimeter values obtained with the other controllers. The three controllers show similar energy consumption over time.

	LQR	**MPC**	**MPC Offset-free**
mean(Δp)	0.8892	0.6867	0.6168
mean(Δv)	0.3987	0.2611	0.2522
IAE on Δp	13.2352	10.1978	9.1515
IAE on Δv	5.9811	3.9176	3.7826
min(Δp)	1.1885	2.2371	2.3605
Energy consumption	0.5208	0.5200	0.5207
Steady state error	0.1354	0.1079	0.0009
"Rise" time to d_{des}	3.3	3.75	3.85

Table 3.3: Comparison of controllers performance: Ta Lou velocity profile

3.3 Test on men velocity profile of Coleman

It is reasonable that by intensifying the difficulty of the velocity profile from the one of a female runner to the one of male, the required initial distance from the go-kart is going to increase. In the case of the Christian Coleman velocity profile this value is set to $\bar{d} = 13$ meters.

When intializing the maneuver from a further distance compared to the previous scenario, higher values of mean position error and Integral Absolute Error observed, as reported in Table 3.4. The value of the minimum distance reached between

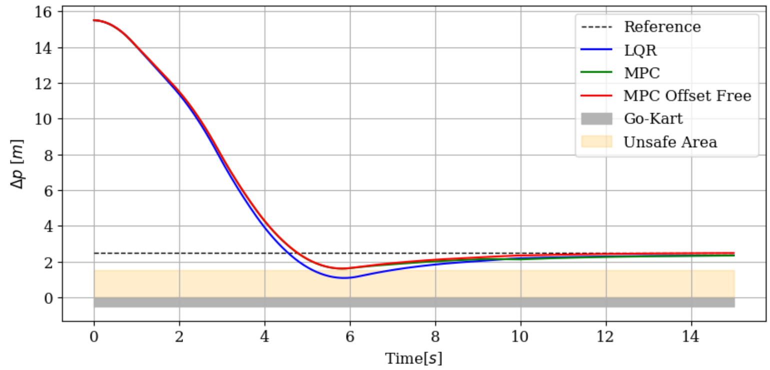

(a) Relative position between runner and go-kart

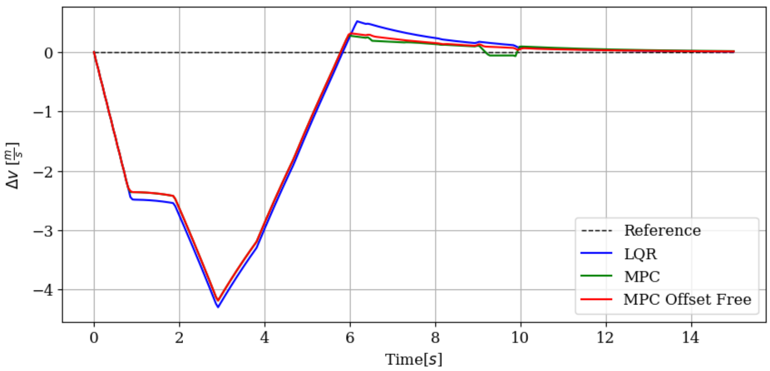

(b) Relative velocity between runner and go-kart

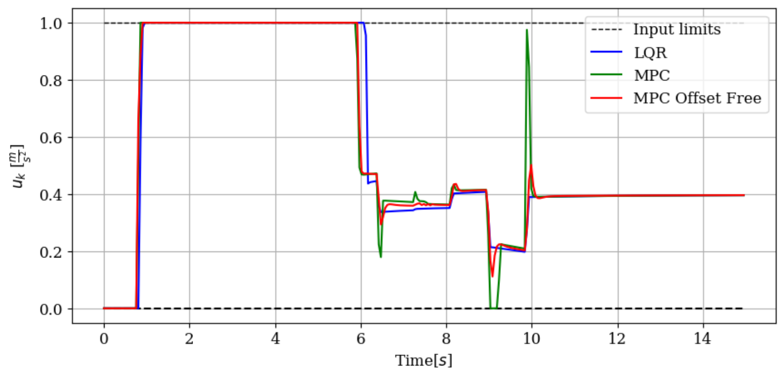

(c) Input effort (drive-train acceleration)

Figure 3.3: Simulation results following Coleman velocity profile. The results for LQR (in blue), MPC (in green) and Offset-free MPC (in red) are shown overlapped on the same plot to appreciate the comparison among controllers

runner and go-kart is much smaller for the LQR with respect to the two MPC formulations also in this simulation, meaning that the athlete enters for a bigger

	LQR	**MPC**	**MPC Offset-free**
mean(Δp)	2.5984	2.5636	2.4848
mean(Δv)	1.0037	0.9392	0.9419
IAE on Δp	38.6465	38.1247	36.9459
IAE on Δv	15.0578	14.0901	14.1308
min(Δp)	1.0802	1.6036	1.6105
Energy consumption	0.5694	0.5694	0.5697
Steady state error	0.1689	0.1784	0.0350
"Rise" time to d_{des}	4.5	4.7	4.7

Table 3.4: Comparison of controllers performance: Coleman velocity profile

distance inside the shield. The recorded LQR value of 1 meter and 8 centimeters violates the safety bound introduced in the MPC, similar to the observation made in the Ta Lou velocity profile case. Furthermore, it's worth noting that the offset-free MPC consistently outperforms both LQR and MPC in terms of steady-state error, achieving the lowest value among the three controllers.

It should be noticed that, in both the scenario saturation phenomenon is present for a consistent part of the tracking with the LQR controller.

3.4 Disturbance observer results

In this section the output of the disturbance observer and state estimator formulated in (2.26) is shown. Figure 3.4

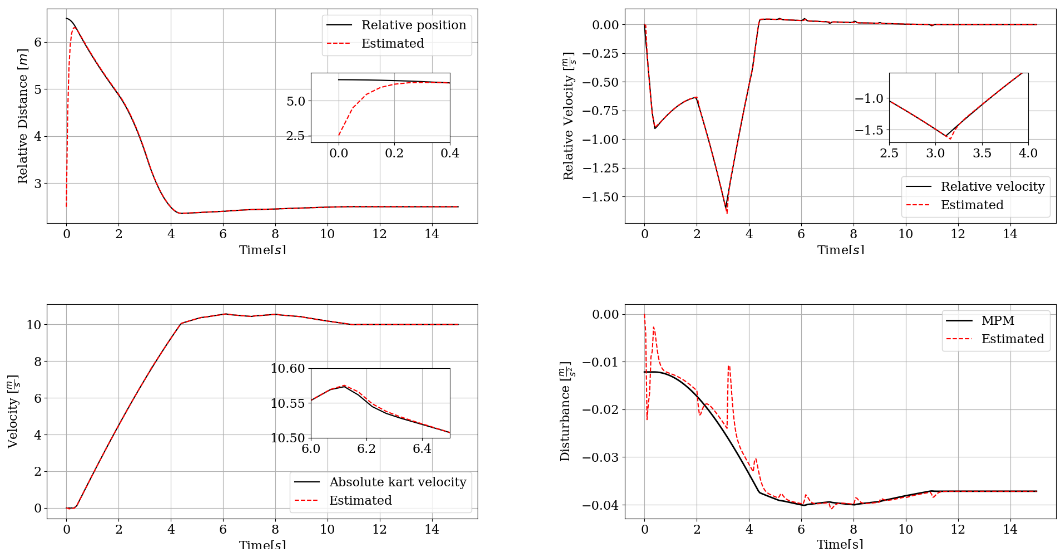

Figure 3.4: Estimated state variables and observed Model-Plant mismatch term, compared to real known values

Chapter 4

System Structure and Hardware-in-the-loop implementation and results

In this chapter an overview of the hardware structure and sensors equipment of the system is provided together with the changes in the controllers formulations with respect to the simulation environment. Later, an overview of the technologies studied and used for the implementation on the hardware of the control algorithms. Finally, some test developed on the real hardware are presented and their results are shown and analyzed.

4.1 System structure

This part discuss the hardware components present in the system.

The system comprises a fully electric-powered go-kart with an attached airshield structure via a fixed joint. According to the CIK-FIA (International Karting Commission Federation International Automobile), a go-kart is a land vehicle with four non-aligned wheels in contact with the ground, two of which control steering while the others transmit power. Go-karts emerged after the post-war period of the 1950s, originally created by airmen as a pastime. Typically, go-kart chassis are constructed from steel pipes that provide both stiffness and flexibility to compensate for the lack of a suspension system and a differential.

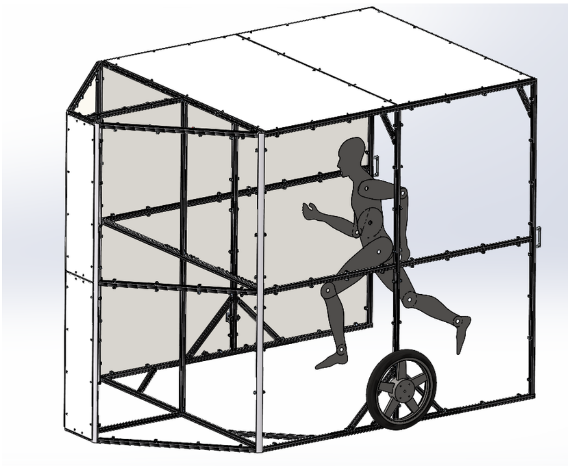

Figure 4.1: Airshield structure

Electric-powered go-kart

The kart is a SinusIon purchased from the German company RiMO (originally Richter + Mohn).

The battery on board is a lithium-iron-manganese-4-phosphate (LiFeMnPO4), used in order to reduce the battery pack weight.

For what regards the motor it's a Heinzmann PMS 100, with air-cooled cooling technology. This DC motor is a permanent magnet brush-less motor with a link voltage of 28V, a nominal speed of 6500 rpm and a rated torque of 3.82 Nm, representing respectively the rotational speed at which the motor is designed to operate optimally and the maximum rotational force that the motor can exert. Talking about efficiency this motor is characterized with high-efficiency and energy-saving capabilities, the rated power output is 2.6kW. This parameter reflects the motor's ability to convert electrical energy into mechanical power. The gearbox has a gear ratio of 1:7.

The computer on board is a AMD Ryzen MinisForum EliteMini X500 with an AMD Ryzen 7 5700G processor (8 cores with nominal frequency of 3.8GHz) coupled with a 16GB DDR4 RAM.

Airshield

The shield has the structure shown in 4.1. All the side and front panels are of plexiglass while the top part is an aluminium composite.

Height	2.15 m
Width	1.86 m
Lenght	2.95 m

Table 4.1: Aishield dimensions

The dimensions are reported in table 4.1.

The height can be adjusted inside a range of circa 13 cm by simply moving a wheel bracket up or down, in order to better fit the height of the runner.

4.2 Perception

Autonomous vehicles sense and perceive the surrounding environment using measurements coming from sensors and then process the information in order to make informed decisions. This is the fundamental principle behind closed loop control that relies on measurements of controlled variables, provided by an appropriate sensor. The perception systems used in autonomous vehicles are usually categorized in two groups:

- Proprioceptive sensors (or internal state sensors) sensing the vehicle own state like wheel encoders or inertial measurement unit, location sensors like GPS, etc.
- Exteroceptive sensors (or external state sensors) gathering informations about the surrounding environment like cameras, LiDAR, RADARs, etc.

In this application the system is equipped with a LiDAR (Light Detection and Ranging), a camera, an inertial measurement unit and wheel encoders.

LiDAR

LiDAR (Light Detected and Ranging) is a remote sensing technology that measures distances to objects and surfaces using laser pulses. The sensor consists of three main components: a laser emitter, a scanning mechanism, and a receiver. The laser emitter sends out short pulses of laser light, which travel towards surrounding objects. When these pulses encounter an object they reflect off its surface and return to the LiDAR sensor. The receiver than detects the reflected light and measures the time it takes for the pulses to return, allowing to calculate the distance of the object based on the speed of light. Moreover, LiDAR rensors are capable of operating in various environmental conditions including darkness, rain, fow or low visibility, making them perfect for the application and highly reliable.

The LiDAR mounted on the airshield is a Velodyne VLP-16, a compact sensor that features 16 laser channels arranged in a circular configuration to have an important field of view.

The field of view (angular extension of a scene that is projected by the laser beam) is of 360° horizontal and 30° vertical. The range of the laser is up to 100 m. Measures have an accuracy of +/- 3 cm and are acquired with a frequency of 20 Hz.

Camera

Cameras provide rich information about the surrounding environment and can be used in a variety of ways. On the airshield a ZED 2i Stereo Camera with polarized lens of 4mm is mounted.

The field of view is of 120° and the camera is able to sense ranges between 1.5 m and 35 m. The depth accuracy is smaller of the 2% of the distance up to 10 m while it increases up to the 7% for distances up to 30m distance.

The camera is equipped with a Stereolab ZED Box Xavier NX 8GB, an industrial compact and powerful mini PC used for computing and processing camera data. It's powered with an NVIDIA Jetson embedded GPU.

At the moment LiDAR measurement are prefered with respect to camera ones thanks to the higher accuracy. Camera remains responsible for the detection of the gesture to identify the moment in which the runner is able to start the performance.

Wheel Encoder

Rotary encoders are a type of sensor that measures the rotation of a mechanical shaft. Two wheel encoders, one for each wheel, are integrated in the PMS 100 motor as speed sensors providing the motor rotational speed. Then by knowing that the gear ratio is 1:7 and that the wheel diameter is 27.89 cm the absolute go-kart speed can be evaluated as follows:

$$v_{\text{kart}} = \frac{\pi \cdot d \cdot \text{avg rate}}{60 \cdot \text{gear ratio}} \tag{4.1}$$

where avg rate is the average motor rate between left and right sides.

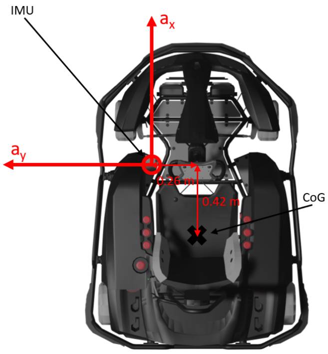

Figure 4.2: IMU position on the go-kart

Inertial Measurement Unit

Typically an IMU or Inertial Measurement Unit consists of a combination of accelerometers and a gyroscopes, and sometimes also magnetometers in order to measure the orientation, velocity and acceleration of an object. Thanks to the combination of accelerometers and gyroscopes the IMU is able to sense the object orientation or angular motion and acceleration with respect to some predefined axes. The IMU used in the go-kart is the IRIMU-V2 from Izze-Racing that outputs data at 200Hz via CAN protocol and has an accuracy of less than 1% of full scale for the acceleration and less than 1.5% for the angular acceleration. The position with respect to the go-kart centre of gravity is showed in 4.2.

4.3 Controller design changes for hardware integration

In the context of the hardware control implementation the available informations are the one coming from sensors and we cannot rely on a full state knowledge for both runner and kart as hypotized in Chapter 2. For this reason we have to take into account the sensor present in the system and the measurement provided by them to control the system properly.

LQR

Differently from the simulation context, where all the state variables both for runner and kart have been considered to be fully known, in the hardware-in-the-loop context, absolute position of both kart and runner, as well as the runner absolute velocity, result to be unknown.

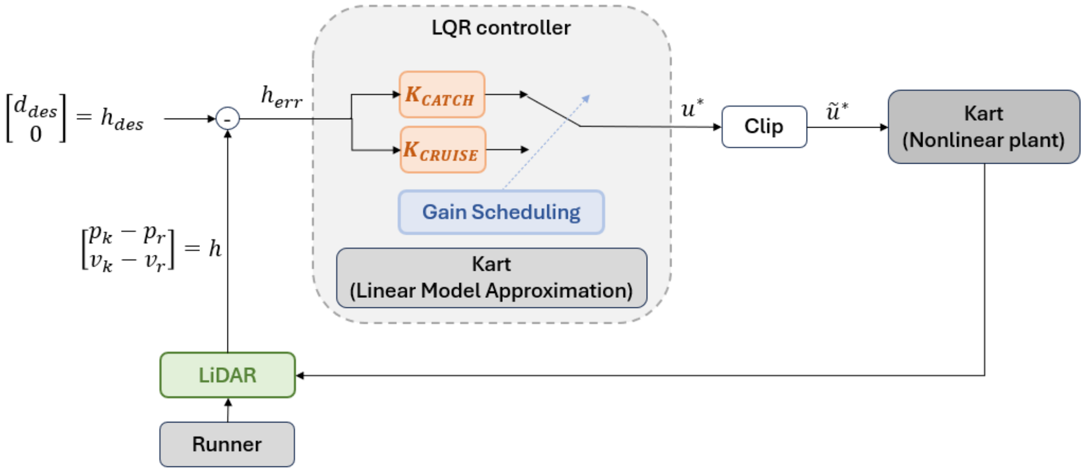

Figure 4.3: Linear Quadratic Regulator scheme with sensors

The LiDAR, as a range sensor, provides directly the measurement of the relative distance between runner and kart Δp, while the relative velocity can be estimated via finite differences:

$$\Delta v_t = \frac{\Delta p_t - \Delta p_{t-1}}{dt} \tag{4.2}$$

where $\Delta p_t := p_{k,t} - p_{r,t}$ and $\Delta v_t := v_{k,t} - v_{r,t}$, and dt is the sampling time.

The third component of the prediction state, the kart absolute velocity, is obtained from the wheel encoders.

The closed loop control law in 1.8 can be modified as follows to directly use the measurments provided by the LiDAR to evaluate the feedback error and compute the current control action:

$$u_t^* = K(h_t - h_{\text{des}}) \tag{4.3}$$

where

$$h_t = \begin{bmatrix} \Delta p_t \\ \Delta v_t \end{bmatrix} = \begin{bmatrix} p_{k,t} - p_{r,t} \\ v_{k,t} - v_{r,t} \end{bmatrix}, \quad h_{\text{des}} = \begin{bmatrix} d_{\text{des}} \\ 0 \end{bmatrix}. \tag{4.4}$$

MPC

The overall implementation of the LQR in the context of the real system in described by algorithm 4, while the control architecture using the sensors for taking the measurements is shown in figure 4.4.

It has to be noticed that the actual absolute runner acceleration is estimated. First of all the relative acceleration between kart and runner Δa is estimated, as

Algorithm 4 LQR implementation on hardware system

```
catched = false;
Set initial runner position with a proper distance d̄ from kart;
Define desired system behaviour h_des = [d_des, 0]^T;
for t = 0, 1, 2, ... do;
    Take LiDAR information h_t = [Δp_t, Δv_t]^T;
    Take absolute kart velocity v_{k,t} from wheel encoders;
    Evaluate absolute runner velocity v_{r,t} = v_{k,t} − Δv_t;
    if v_{k,t} ≥ 0.8 v_{r,t} and catched = false then
        catched = true;
    end if
    if catched = false then
        u* = −K_catch(h_t − h_des);
    else
        u* = −K_reg(h_t − h_des);
    end if
    Clip input according to limit saturation limits ũ* = sat_[a_min, a_max](u*);
    Inject ũ* in the plant;
end for
```

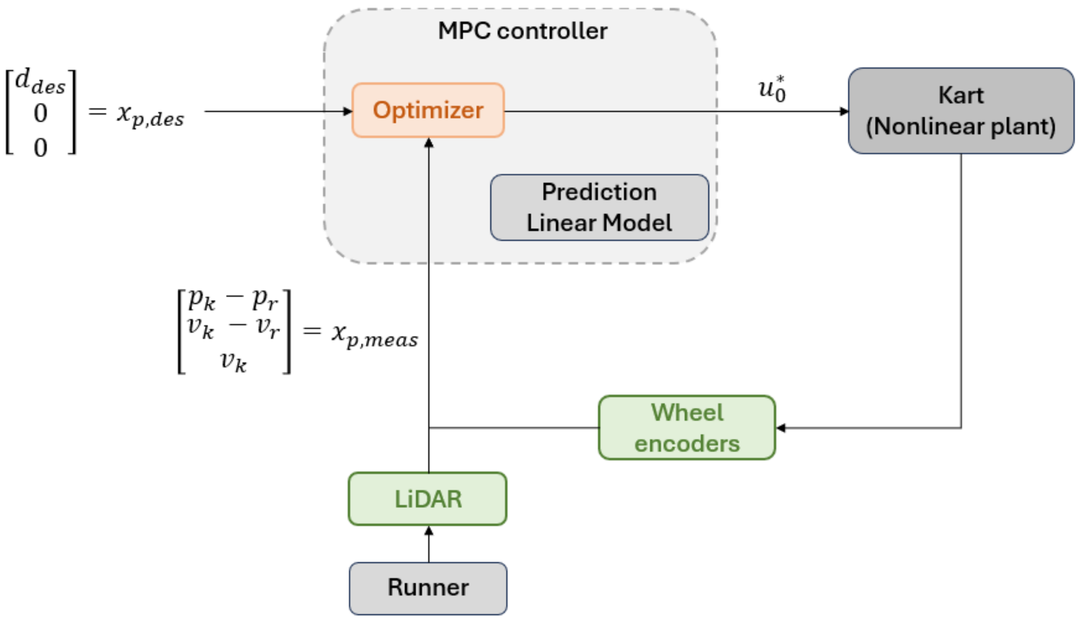

Figure 4.4: Model Predictive Control scheme with sensors

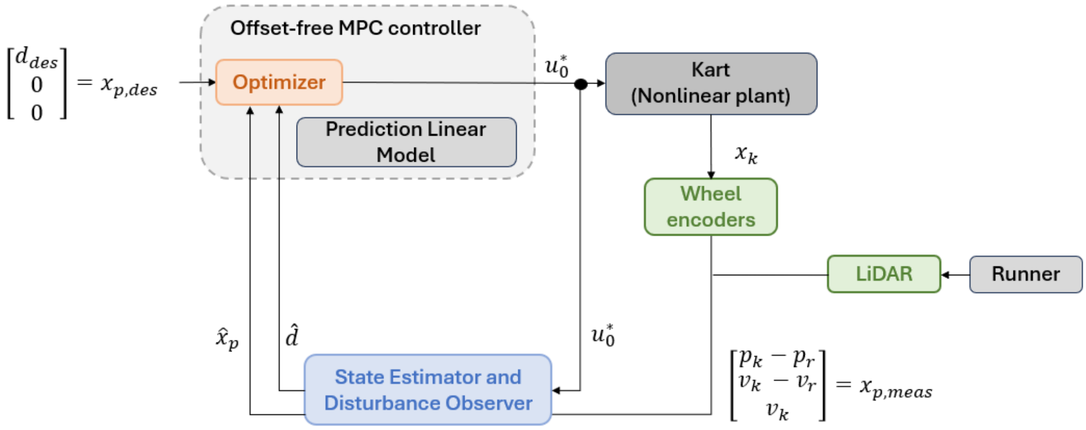

Figure 4.5: Offset-free Model Predictive Control scheme with sensors

well as the kart absoluted acceleration a_k. The absolute runner acceleration used is equal to $a_r = a_k - \Delta a$. For this purpose a Kalman filter has been used.

Tutto il discorso sul noise

Offset-free MPC

4.4 Experimental tools

In this paragraph the tools used for the development of the controllers implementation on the system are briefly presented.

Robot Operating System

Robot Operating System (ROS) is an open-source middleware framework specifically designed for robotics research and development [19] of robotic applications. Despite the name it is not a real operating system but it's a collection of libraries, tools and conventions that allows robotic developers to share, re-use and manage the applications. Being a communication and middleware layer it serves as an important intermediary layer between the operating system and software applications. One of the key features of ROS is its modular architecture, which promotes code reuse and modularity by breaking down robot applications into smaller, reusable components called "nodes." A node is an individual specific and independent program written in Python or C++ that executes a specific task or function within the framework of a more complex application. The nodes can communicate with each other using a publish-subscribe messaging system, allowing for flexible and decentralized control

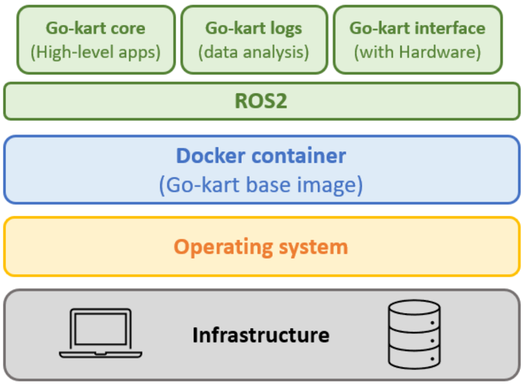

Figure 4.6: Docker

architectures. In particular nodes can publish messages to topics (publisher) and other nodes can subscribe to these topics to receive and process the data (suscriber).

ROS, and in particular its successor ROS2, offers numerous features and improvements that make it well-suited for driving autonomous systems and automated driving projects. At the core of ROS2's functionality lies the ability to run directly on the onboard computer of autonomous systems, having Ubuntu pre-installed, processing sensors raw data coming from sensors, processing them and executing the proper control algorithms. In this sense, one of the most notable innovations in ROS2 is its ability to support real-time capabilities, of fundamental importance when autonomous systems have to perform safety-critical and time-sensitive applications.

Docker

Docker is an open-source platform that enables developers to package, distribute, and run applications in lightweight, portable containers. These containers encapsulate all the dependencies and runtime components needed to run an application, including the code, system tools, libraries, and settings. Docker containers are designed to be isolated from each other and from the underlying host system, ensuring consistent and reliable execution across different environments. The only thing preventing a container from being able to stand alone is that it relies on the host's operating system (OS) and kernel for low-level services, such as resource management and network access.

Go-kart repository

The autonomous go-kart repository consists of four different images. The first one is the Ubuntu 20.04 base image with ROS2 installed and is the base for the other go-kart repositories stack. This layer manages the installation of the common libraries and the ROS2 communication between the hardware components (sensors and actuators) and the software applications contained in the other three higher-level images. The communication is achieved through the ad-hoc definition of messages.

The go-kart logs is the repository responsible for data analysis. Specifically, it interprets and decodes binary sensor data into a numerical format that is meaningful and can be understood and processed by other software applications, such as control algorithms. In this application, binary signals are converted into CSV files.

The go-kart interface repository is responsible for interfacing with hardware, serving as the intermediary layer between the operating system and the hardware. Drivers read messages from ROS topics, enabling hardware components (such as LiDAR, cameras, motors, etc.) to execute requested actions.

Finally, the go-kart core contains all the high level applications, such as the controller. Several C++ packages for estimation, control, or visualization exist in order to execute various tasks in a modular and reusable manner.

4.5 Hardware-in-the-loop implementation and tests

In this section some hardware-in-the-loop tests developed are presented and analyzed.

Figure 4.7: Sequence of images taken from a video, showing a catch-up maneuver regulated with MPC

Figure 4.8: Sequence of images taken from a video, showing a tracking regulated with MPC

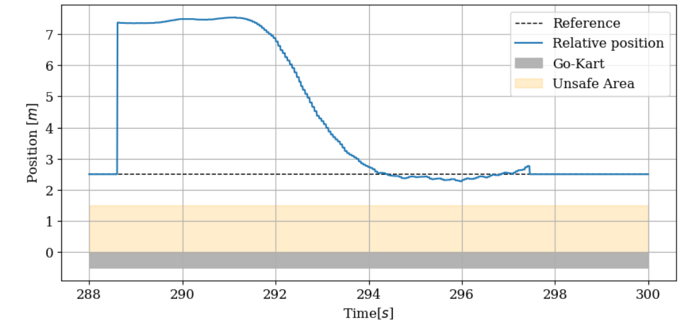

(a) Relative position between runner and go-kart

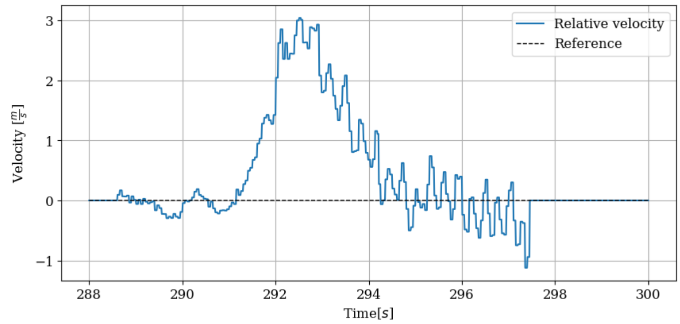

(b) Relative velocity between runner and go-kart

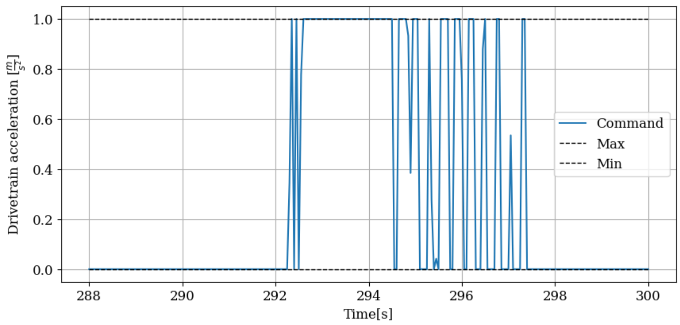

(c) Input effort (drive-train acceleration)

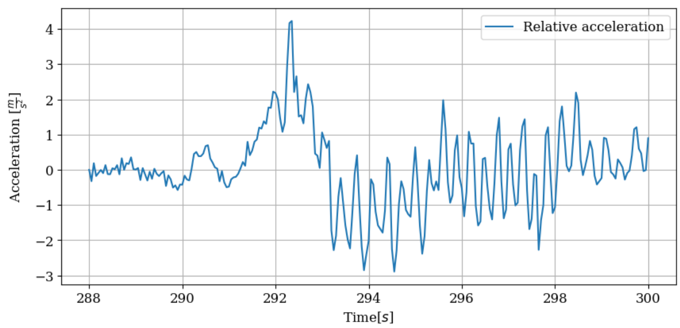

(d) Estimated Acceleration

Figure 4.9: Hardware tests results

Bibliography

[1] H. Müller and B. Glad, "Technology in athletics," *Journal of Sports Science*, 2014.

[2] R. J. Corn and D. Knudson, "Effect of elastic-cord towing on the kinematics of the acceleration phase of sprinting," *Journal of Strength and Conditioning Research*, vol. 17, no. 1, pp. 72–75, 2003.

[3] W. P. Ebben, J. A. Davies, and R. W. Clewien, "Effect of the degree of hill slope on acute downhill running velocity and acceleration," *Journal of Strength and Conditioning Research*, vol. 22, no. 3, pp. 898–902, 2008.

[4] CONI. "Presentato lo scudo aerodinamico, l'arma in piú al servizio dell'atletica." (2021), [Online]. Available: `https://www.coni.it/it/news/18045-presentato-lo-scudo-aerodinamico,-l-arma-in-piu-al-servizio-dell-atletica.html`.

[5] S. E. S. D. Director, "Review of the state of development of advanced vehicle control systems (avcs)," *Vehicle System Dynamics*, vol. 24, no. 6-7, pp. 551–595, 1995.

[6] K. Yi, J Hong, and Y. Kwon, "A vehicle control algorithm for stop-and-go cruise control," *School of Mechanical Engineering, Hanyang University, Seoul, Korea; Hyundai Motor Company, Kyonggi-Do, Korea*, 2001.

[7] D. Mayne, J. Rawlings, C. Rao, and P. Scokaert, "Constrained model predictive control: Stability and optimality," *Automatica*, vol. 36, no. 6, pp. 789–814, 2000, ISSN: 0005-1098.

[8] W. Lim, S. Lee, J. Yang, M. Sunwoo, Y. Na, and K. Jo, "Automatic weight determination in model predictive control for personalized car-following control," *IEEE Access*, vol. 10, pp. 19 812–19 824, 2022.

[9] G. Naus, R. van den Bleek, J. Ploeg, B. Scheepers, R. van de Molengraft, and M. Steinbuch, "Explicit mpc design and performance evaluation of an acc stop-&-go," in *2008 American Control Conference*, 2008, pp. 224–229.

[10] G. Pannocchia, "Offset-free tracking mpc: A tutorial review and comparison of different formulations," in *2015 European Control Conference (ECC)*, 2015, pp. 527–532.

[11] U. Maeder, F. Borrelli, and M. Morari, "Linear offset-free model predictive control," *Automatica*, vol. 45, no. 10, pp. 2214–2222, 2009, ISSN: 0005-1098.

[12] A. Radke and Z. Gao, "A survey of state and disturbance observers for practitioners," in *2006 American Control Conference*, 2006.

[13] R. E. Kalman *et al.*, "Contributions to the theory of optimal control," *Bol. soc. mat. mexicana*, vol. 5, no. 2, pp. 102–119, 1960.

[14] D. Hu, G. Li, G. Zhu, Z. Liu, and M. Tu, "Linear-quadratic tracking control of a commercial vehicle air brake system," *IEEE Access*, vol. 8, pp. 149 741–149 750, 2020.

[15] G. Pannocchia and J. B. Rawlings, "Disturbance models for offset-free model predictive control," *AIChE J.*, vol. 49, pp. 426–437, 2003.

[16] *Diamond league homepage*, `https://www.diamondleague.com/home/`, Accessed: February 26, 2024.

[17] S. Diamond and S. Boyd, *Cvxpy: A python-embedded modeling language for convex optimization*, 2016. eprint: `1603.00943`.

[18] B. Stellato, G. Banjac, P. Goulart, A. Bemporad, and S. Boyd, "Osqp: An operator splitting solver for quadratic programs," *Mathematical Programming Computation*, vol. 12, no. 4, 637–672, Feb. 2020, ISSN: 1867-2957.

[19] M. Quigley, K. Conley, B. Gerkey, *et al.*, "Ros: An open-source robot operating system," in *ICRA workshop on open source software*, Kobe, Japan, vol. 3, 2009, p. 5.